Cardioprotective c-kit+ cells are from the bone marrow and regulate the myocardial balance of angiogenic cytokines

Shafie Fazel,[1] Massimo Cimini,[1] Liwen Chen,[1] Shuhong Li,[1] Denis Angoulvant,[1] Paul Fedak,[1] Subodh Verma,[2] Richard D. Weisel,[1] Armand Keating,[3] and Ren-Ke Li[1]

[1]Division of Cardiovascular Surgery, Toronto General Hospital, [2]St. Michael's Hospital, and [3]Department of Medical Oncology and Hematology, Princess Margaret Hospital and Ontario Cancer Institute, University Health Network, University of Toronto, Toronto, Ontario, Canada.

Clinical trials of bone marrow stem/progenitor cell therapy after myocardial infarction (MI) have shown promising results, but the mechanism of benefit is unclear. We examined the nature of endogenous myocardial repair that is dependent on the function of the c-kit receptor, which is expressed on bone marrow stem/progenitor cells and on recently identified cardiac stem cells. MI increased the number of c-kit+ cells in the heart. These cells were traced back to a bone marrow origin, using genetic tagging in bone marrow chimeric mice. The recruited c-kit+ cells established a proangiogenic milieu in the infarct border zone by increasing VEGF and by reversing the cardiac ratio of angiopoietin-1 to angiopoietin-2. These oscillations potentiated endothelial mitogenesis and were associated with the establishment of an extensive myofibroblast-rich repair tissue. Mutations in the c-kit receptor interfered with the mobilization of the cells to the heart, prevented angiogenesis, diminished myofibroblast-rich repair tissue formation, and led to precipitous cardiac failure and death. Replacement of the mutant bone marrow with wild-type cells rescued the cardiomyopathic phenotype. We conclude that, consistent with their documented role in tumorigenesis, bone marrow c-kit+ cells act as key regulators of the angiogenic switch in infarcted myocardium, thereby driving efficient cardiac repair.

Introduction

Initial data from rodent studies suggested that either direct implantation of c-kit+ hematopoietic stem cells into infarcted myocardium or their mobilization by SCF (ligand for c-kit) and G-CSF at the time of myocardial infarction (MI) could lead to robust cardiomyocyte regeneration and restoration of cardiac function (1, 2). These studies sparked several clinical trials of bone marrow cell therapy after MI, which in general have shown promising results (3). More recently, transdifferentiation of HSC to cardiomyocytes has been challenged, calling into question the very rationale that guided the design of these trials (4–6). In order to gain insight into the potential mechanism of benefit of cellular therapy, we sought to characterize the endogenous cardiac repair responses that involve the c-kit/SCF pathway. Understanding these mechanisms may facilitate the rational design of future biointerventions aimed at alleviating the burden of acquired cardiovascular diseases that remain the leading cause of death in the Western world.

The protooncogene *c-kit*, which encodes a receptor tyrosine kinase, maps to the W locus and is important for gametogenesis, melanogenesis, and hematopoiesis (7). Although no cardiac anomaly is noted in mice bearing mutations in the *c-kit* or *SCF* genes, the c-kit protein has been shown to be expressed on the cell surface of putative adult cardiac stem cells (8). Within the bone marrow, c-kit is expressed on hemangioblasts, which are the precursor to HSCs as well as the endothelial progenitor cells (EPCs) (9, 10). EPCs were first identified as a subset of $CD34^+CD45^+$ PBMCs that also expressed VEGFR2 (11). These cells were shown to attach to fibronectin and adopt an endothelial cell–like phenotype. Both the HSCs and EPCs continue to express c-kit into adulthood (12). Although SCF is not important for the generation of c-kit+ HSCs, it has been shown to be critical for their mobilization into peripheral circulation (13, 14). Indeed, mice with mutations in the c-kit receptor are poor HSC mobilizers (15). In accordance with this data, it is speculated that a similar mechanism of EPC mobilization requiring c-kit signaling occurs in response to tissue ischemia (16, 17).

The role of bone marrow resident c-kit+ cells in organ repair has not been previously investigated. However, bone marrow–derived c-kit+ cells have been implicated in tumor angiogenesis. Specifically, trafficking of c-kit+ cells to tumors is associated with the onset of angiogenesis, and absence of such trafficking in c-kit mutant mice is associated with diminished angiogenesis even in the face of forced carcinogenesis (18, 19). Similarly, depletion of c-kit+ cells with c-kit–specific antibody blocks tumor angiogenesis (20). These roles are consistent with an absence of an EPC response when c-kit is mutated or blocked, although this remains speculative.

Based on the foregoing discussion, we hypothesized that the role of the bone marrow resident c-kit+ cells in endogenous cardiac repair is likely to involve the post-MI angiogenic pathways. To address this hypothesis, we used the compound heterozygous c-kit mutant Kit^W/Kit^{W-v} mouse, which has a relatively normal lifespan and is the only c-kit mutant in which HSC mobilization has been previously shown to be defective in spite of relatively normal numbers of HSCs (15). The W mutation is the result of a 78–amino acid deletion that includes the transmembrane domain of the c-kit protein, and the W-v mutation is a missense mutation in the kinase domain of the c-kit coding sequence (21). We postulate that EPC mobilization is also defective in these mice after MI. In support of this postulate, we show that the majority of c-kit+ cells that are recruited to infarcted myocardium are from

Nonstandard abbreviations used: EPC, endothelial progenitor cell; MI, myocardial infarction; PCNA, proliferating cell nuclear antigen.

Conflict of interest: The authors have declared that no conflict of interest exists.

Citation for this article: *J. Clin. Invest.* **116**:1865–1877 (2006). doi:10.1172/JCI27019.

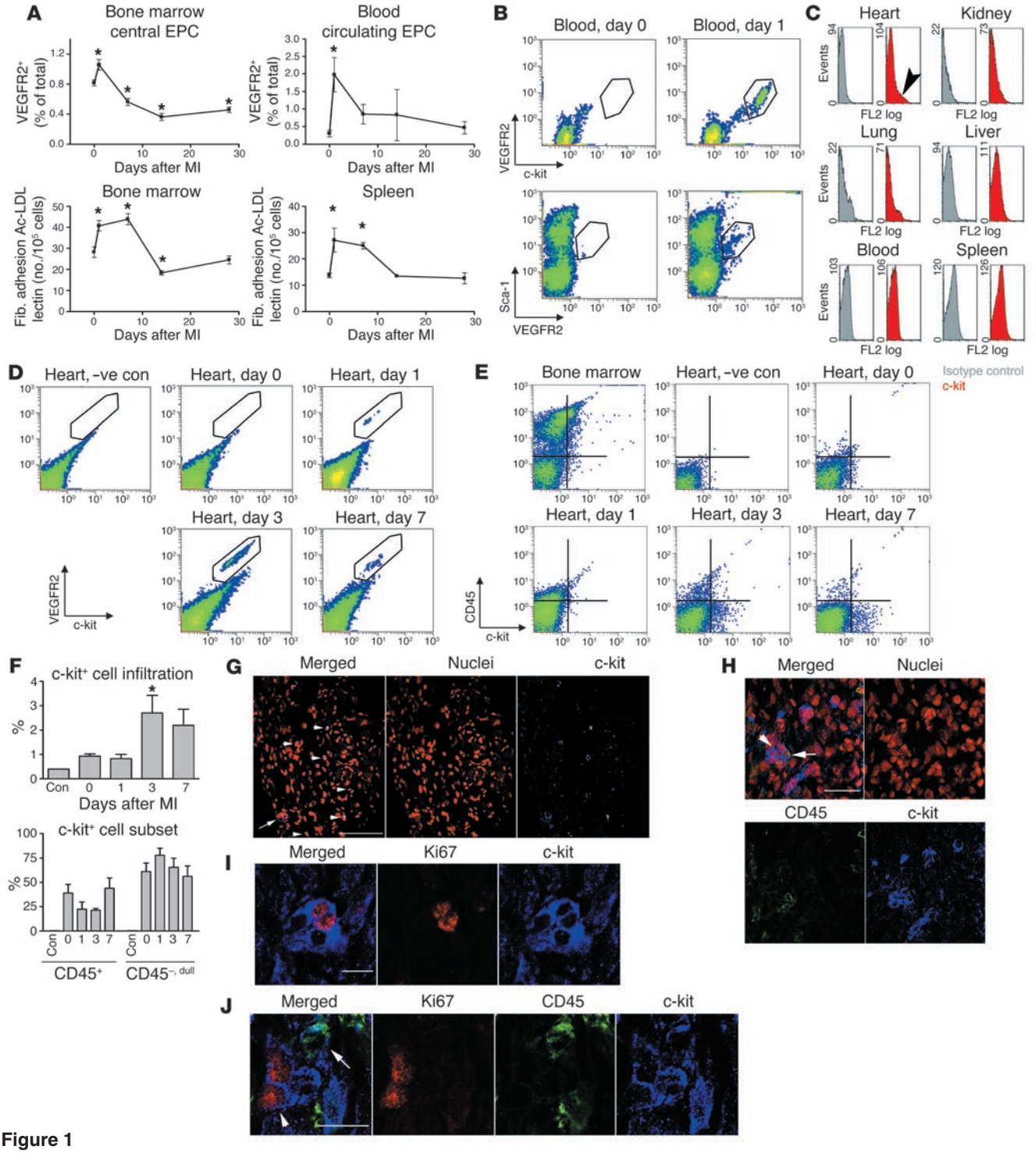

Figure 1

c-kit+ cells increase in infarcted myocardium. (**A**) Quantification of EPCs over a time course after MI in wild-type mice. Upper panels, flow cytometry for VEGFR2+ cells. Lower panels, in vitro splenocyte fibronectin (Fib.) adhesion, acetylated LDL uptake (Ac-LDL), and lectin-binding assay results. Total number of cells was calculated by multiplying percentage of positive cells by total number of cells isolated from both tibia and femur of 1 mouse. $n = 3–5$ per time point. *$P < 0.05$ compared to day 0 values. (**B**) MI causes an increase in VEGFR2+c-kit+Sca-1+ subset of PBMCs. (**C**) Increase of c-kit+ cells is specific to the injured myocardium (arrowhead). Seven days after MI, c-kit+ cells were not detected in other organs and the peripheral circulation. Gray, isotype control; red, c-kit. (**D** and **E**) The c-kit+ cells detected after MI in the heart were homogeneously VEGFR2+ but heterogeneous with respect to CD45 expression. –ve con, negative control. (**F**) Quantification of the number of c-kit+ cells. Lower panel shows that the majority of the c-kit+ cells in the heart were CD45−. $n = 3$ per time point. (**G**–**J**) Confocal microscopic images. (**G**) c-kit+ cells visualized at the infarct border zone both as isolated cells (arrowheads) and in clusters (arrow). Scale bar: 100 μm. (**H**) The majority of the c-kit+ cells did not express CD45 (arrowhead) although some of the clusters contained CD45-expressing cells (arrow). Scale bar: 50 μm. (**I**) c-kit+ cells present in the clusters are shown to express Ki67 cell cycling–associated nuclear antigen. Scale bar: 10 μm. (**J**) c-kit+ cells in the cell cycle (arrowhead) did not coexpress CD45 (arrow). Scale bar: 10 μm.

the bone marrow and require c-kit function for their mobilization. We also show that abnormality in the c-kit/SCF pathway leads to dilated cardiomyopathy and death from cardiac failure. Finally, we show that failing Kit^{W}/Kit^{W-v} hearts are rescued with bone marrow replacement from wild-type mice and that the endogenous role of the bone marrow c-kit$^+$ cells is to promote the angiogenic switch in infarcted myocardium by regulating the myocardial angiogenic cytokine milieu.

Results

c-kit$^+$ cells increase in infarcted myocardium. The kinetics of EPC distribution after MI was assessed after coronary ligation in wild-type mice. Fibronectin-adherent endothelial-like cell numbers increased in both the bone marrow and the peripheral circulation within the first week, with a rapid decline thereafter (Figure 1A). As anticipated, the dynamics of VEGFR2$^+$ cell redistribution in the bone marrow and the PBMCs closely matched these data (Figure 1A). Cell surface phenotyping of the VEGFR2$^+$ cells showed that more than 95% of VEGFR2$^+$ cells also expressed Sca-1 and c-kit (Figure 1B). Thus, coronary ligation leads to a robust increase in the number of peripheral blood VEGFR2$^+$c-kit$^+$Sca-1$^+$ cells, a phenotype that is consistent with previously reported phenotype of EPCs.

After MI, c-kit$^+$ cells could readily be detected in the myocardium that was subtended by the ligated coronary artery (Figure 1, C–F). Seven days after MI, c-kit$^+$ cells could not be detected in noninjured organs: lung, liver, kidney, and the peripheral blood (Figure 1C). Of the c-kit$^+$ cells in infarcted myocardium, more than 95% expressed VEGFR2 (Figure 1D), but only 30% expressed CD45 (Figure 1, E and F). The CD45-expressing cells had 1.2 ± 0.2 fluorescent log units lower CD45 levels than c-kit$^+$ cells in the bone marrow ($P < 0.001$). This finding was independent of the treatment required to release single cells from the heart for flow cytometry (Supplemental Figure 1; supplemental material available online with this article; doi:10.1172/JCI27019DS1). Whether this phenomenon represented preferential proliferation or recruitment of CD45$^-$ cells or CD45 downregulation by CD45$^+$ cells is not clear.

Microscopy extended observations made by flow cytometry. The c-kit$^+$ cells were rarely detected in the heart prior to MI (2 cells in 8 coronal sections from 4 mice). Visualization of the c-kit$^+$ cells in infarcted myocardium showed cells in isolation and in clusters (Figure 1G). Within the clusters, 85% of the c-kit$^+$ cells did not express CD45 (Figure 1H). Nearly 10% of the c-kit$^+$ cells in the clusters also expressed the cell cycle–associated antigen Ki67 (Figure 1I). Of the 26 c-kit$^+$ clusters comprising 134 c-kit$^+$ cells, 21 c-kit$^+$CD45$^+$ cells were scanned, none of which expressed Ki67 cycling antigen (Figure 1J). This data is consistent with the notion that there is preferential proliferation of c-kit$^+$ CD45$^-$ cells. None of the c-kit$^+$ cells within the clusters showed metachromasia with toluidine blue staining or cytoplasmic granular staining with avidin, suggesting that the c-kit$^+$ cells within the c-kit$^+$ clusters are not mast cells. In fact, toluidine blue staining of infarcted myocardium 7 days after coronary ligation showed that at most 9.6 ± 0.7 mast cells were present per 8 μm coronal myocardial section (Supplemental Figure 2). Thus, MI leads to an increase in c-kit$^+$ VEGFR2$^+$ cells, first in the blood and then specifically within the infarcted myocardium, and the majority of these c-kit$^+$ cells are not mast cells.

c-kit$^+$ cells in infarcted myocardium are from the bone marrow. To address whether the c-kit$^+$ cells in infarcted myocardium are from the bone marrow, we engineered GFP bone marrow chimeric mice to track GFP-expressing bone marrow cells. After stable reconstitution, 69% ± 0.4% of bone marrow cells, 94% ± 0.7% of PBMCs, 84% ± 4% of peripheral EPCs (Figure 2A), 70% ± 6% of PBMC VEGFR2$^+$ cells, and 74% ± 1.2% of c-kit$^+$ cells in the bone marrow expressed GFP (Figure 2B and Table 1). Control C57BL/6 mice did not have GFP-expressing cells in the bone marrow, blood, spleen, or heart. Seven days after MI, c-kit$^+$ cells could be identified in the hearts of C57BL/6 mice, and none expressed GFP. In the GFP chimeric mouse, 74% ± 0.6% of the c-kit$^+$ cells in the heart expressed GFP (Figure 1B and Table 1). Confocal microscopy confirmed that c-kit$^+$ cells in the heart also had GFP expression in the chimeric mice (Figure 2C). Of 7 mast cells identified in sections from 2 mice by avidin staining, none showed GFP staining. Thus, the majority of the non–mast cell c-kit$^+$ cells that infiltrate the infarcted heart are from the bone marrow.

Analysis of 28-day engraftment of bone marrow cells in infarcted myocardium in 4 GFP chimeric mice showed that 30 cells of total 3029 nuclei expressed GFP within the infarcted area and the surrounding border zone. None of these GFP$^+$ cells were cardiomyocytes (Figure 2D). Thus, although bone marrow c-kit$^+$ cells traffic to the infarcted heart, they do not significantly engraft over the long term or give rise to new cardiomyocytes in our current model.

c-kit dysfunction is associated with dilated cardiomyopathy after MI. To examine the functional importance of c-kit–expressing cells in cardiac repair, we examined c-kit mutant Kit^{W}/Kit^{W-v} mice and their congenic $Kit^{+/+}$ wild-type littermates. Coronary ligation excluded a similar volume of myocardium from the circulation immediately after ligation (Figure 3A). Similarly, at 24 hours, no difference in the volume of infarcted myocardium was present (Figure 3A). In spite of the similarity within the first 24 hours, Kit^{W}/Kit^{W-v} mice had a 2-fold increase in mortality compared with $Kit^{+/+}$ mice (Figure 3B). Serial echocardiography demonstrated that cardiac systolic function was reduced and the left ventricle was dilated in Kit^{W}/Kit^{W-v} mice (Figure 3C), with nearly maximal differences emerging within 14 days. Invasive pressure-volume measurements (Figure 3D) showed greater end-systolic and end-diastolic volumes and lower ejection fraction in Kit^{W}/Kit^{W-v} mice. Reduced first derivative of pressure during isovolumic contraction (dP/dt max) and relaxation (dP/dt min) coupled with prolonged time constant of isovolumic relaxation (τ) suggested abnormalities in myocardial energetics in Kit^{W}/Kit^{W-v} mice (see Supplemental Table 1 for

Table 1
c-kit$^+$ cells in infarcted myocardium are from the bone marrow

	Day 0		Day 7	
	c-kit (%)	c-kit GFP (%)	c-kit (%)	c-kit GFP (%)
Bone marrow				
C57	7.6 ± 0.4	0.8 ± 0.1	5.3 ± 0.46	0.7 ± 0.03
C57-GFP	3.4 ± 0.15	6.6 ± 0.12	1.5 ± 0.11	4.0 ± 0.12
Heart				
C57	0.13 ± 0.03	0.07 ± 0.02	2.2 ± 0.26	0.08 ± 0.02
C57-GFP	0.13 ± 0.03	0.09 ± 0.03	0.59 ± 0.04	1.62 ± 0.01

Dual-colored flow cytometry of the heart and bone marrow in C57BL/6 mice (C57) and in C57BL/6-GFP bone marrow chimeric mice (C57-GFP) before (Day 0) and 7 days after (Day 7) MI. Results represent percentage of cells that expressed c-kit but not GFP (c-kit) or c-kit and GFP (c-kit GFP). $n = 5$ per group. Representative flow cytometric plots are presented in Figure 2B.

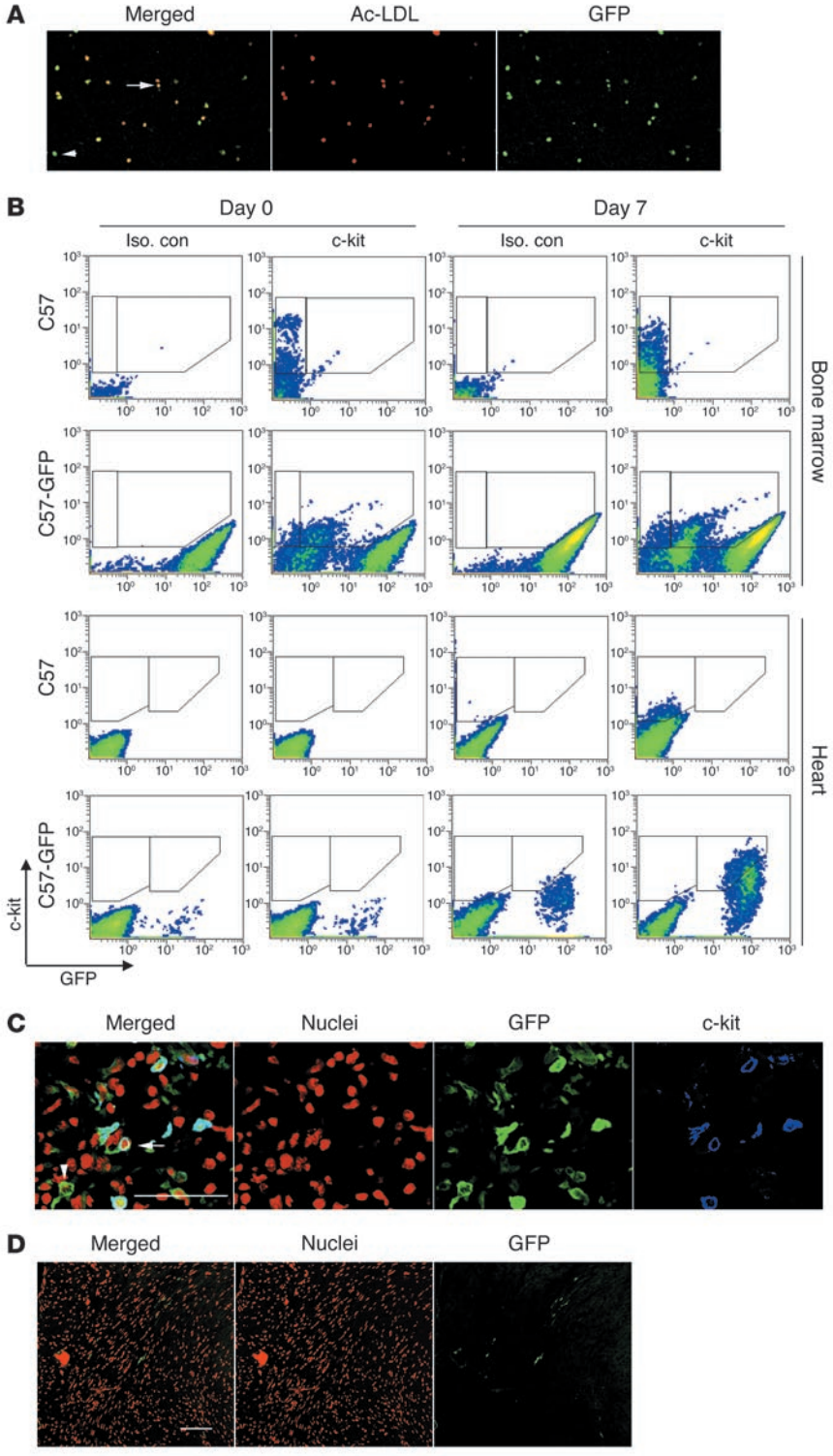

Figure 2
c-kit+ cells in infarcted myocardium are from the bone marrow. (**A**) EPCs from bone marrow chimeric mice carry the GFP transgene. (**B**) Dual-colored flow cytometry of C57BL/6 (C57) or C57BL/6-GFP bone marrow chimeric mice (C57-GFP) for GFP on the *x* axis and c-kit on the *y* axis. In the bone marrow preparation, 74% of c-kit+ cells in the C57-GFP chimeric mice expressed GFP; 74% of c-kit+ cells in the infarcted myocardium in the C57-GFP chimeric mice also expressed GFP. Representative flow cytometry data from 5 independent experiments is shown with results summarized in Table 1. Iso. con, isotype control (**C**) Confocal micrograph confirming that c-kit+ cells in infarcted myocardium also expressed GFP in chimeric mice (arrow). A GFP+ cell that did not express c-kit (arrowhead) is also visualized in this micrograph. Scale bar: 50 μm. (**D**) Engraftment of bone marrow–derived cells was minimal when evaluated at 28 days after MI in the bone marrow chimeric mice. Scale bar: 100 μm.

detailed invasive hemodynamic measurements). Both end-systolic elastance (Ees) and preload recruitable stroke work (PRSW) analysis demonstrated a marked rightward shift of the volume intercept in Kit^{W}/Kit^{W-v} mice (Ees: 2.1 ± 5 μl versus 20.3 ± 5 μl, $P = 0.036$; PRSW: 14.0 ± 3 μl versus 26.0 ± 4 μl, $P = 0.03$), suggesting that the worse cardiac function in Kit^{W}/Kit^{W-v} mice was to a large degree because of exaggerated left ventricular dilation after MI.

Computerized planimetry of explanted hearts fixed at physiologic pressures at 6 weeks also showed 1.8-fold greater left ventricular dilation mainly because of a 2.8-fold greater scar surface area in the Kit^{W}/Kit^{W-v} mice (Figure 3, E and F). The heart to body weight ratio was also 1.2-fold higher in the Kit^{W}/Kit^{W-v} mice, suggesting greater myocyte hypertrophy, which was confirmed by histologic evaluation of cardiomyocyte cross sectional diameter (see Supplemental Table 2 for detailed histomorphometric measurements). These measurements are consistent with end-stage cardiac failure in the Kit^{W}/Kit^{W-v} mice after MI. Interestingly, nonischemic wound healing in the ear was not affected in Kit^{W}/Kit^{W-v} mice (Supplemental Figure 3). Taken together, these data indicate abnormalities in ischemic cardiac repair but not in generalized wound healing in the Kit^{W}/Kit^{W-v} mice.

Acute c-kit dysfunction recapitulates the cardiomyopathic phenotype. To ascertain whether the Kit^{W}/Kit^{W-v} cardiomyopathic phenotype is independent of its anemia, we examined the impact of acute c-kit inhibition in mice treated with Gleevec and in mice rendered acutely anemic by normovolumic hemodilution. Hemodilution nonsignificantly reduced *dP/dt* max and ejection fraction but did not contribute to ventricular dilation. Treatment with Gleevec markedly reduced *dP/dt* max and ejection fraction and led to rapid ventricular dilation after MI. Gleevec also reduced myocardial VEGF and proliferating cell nuclear antigen (PCNA) levels (Supplemental Figure 4). Thus, acute inhibition of c-kit partially recapitulates the functional defects seen in the Kit^{W}/Kit^{W-v} mice.

c-kit dysfunction causes hyporesponsiveness in c-kit+ cells. To confirm the attenuated c-kit function in Kit^{W}/Kit^{W-v} mice in vitro, we har-

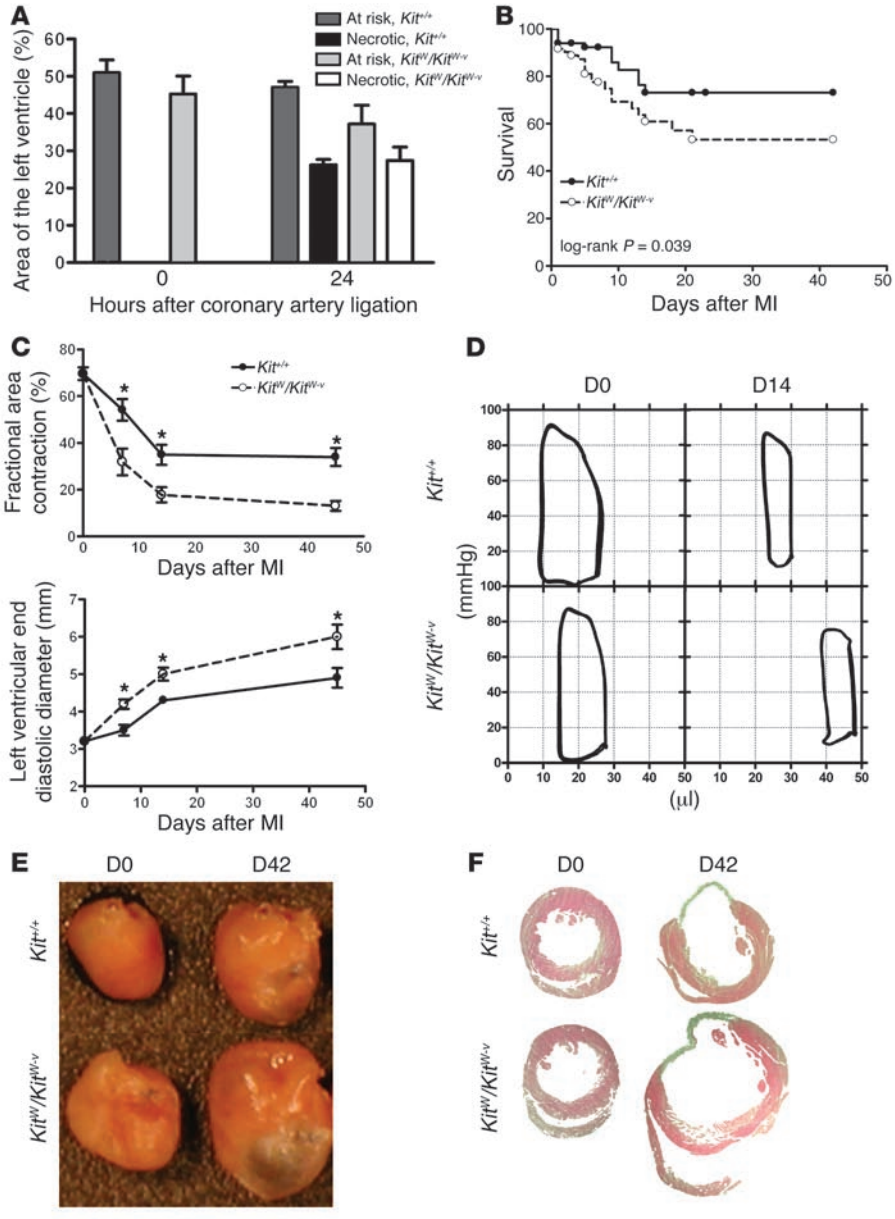

Figure 3
c-kit dysfunction is associated with dilated cardiomyopathy after MI. (**A**) Coronary ligation results in a similar volume of myocardium being at risk for infarction and a similar volume becoming necrotic within 24 hours. $n = 3–4$ per group. (**B**) Actuarial survival is worse in the Kit^{W}/Kit^{W-v} mice after coronary ligation. $n = 86$ per group. (**C**) Echocardiography shows rapid decline in cardiac systolic function (fractional area contraction) and rapid ventricular dilation (left ventricular end diastolic diameter in the mutant mice). $n = 5$ per group. $^{*}P < 0.05$. (**D**) Representative pressure-volume loops of uninfarcted (D0) and infarcted (day 14, D14) $Kit^{+/+}$ and Kit^{W}/Kit^{W-v} mice. $n = 5$ per group. Volume is indicated on the *x* axis and pressure on the *y* axis. (**E**) Representative perfusion-fixed hearts before (D0) and 6 weeks after (D42) coronary ligation. Note the ventricular dilation in the Kit^{W}/Kit^{W-v} mouse. $n = 5$ per group. (**F**) Representative H&E-stained mid-papillary transverse myocardial sections depicting the pronounced ventricular dilation and larger infarct size in the Kit^{W}/Kit^{W-v} mice. $n = 5$ per group.

vested bone marrow cells from Kit^{W}/Kit^{W-v} and $Kit^{+/+}$ mice and cultured them in the absence or presence of SCF. Whereas the $Kit^{+/+}$ cell number and size increased over the 7 days in the presence of SCF, the Kit^{W}/Kit^{W-v} bone marrow cells showed neither an increase in cellularity nor an increase in cell size (Figure 4A). Consistent with the in vitro data, although MI increased myocardial SCF expression in both groups of mice (Figure 4B), the few c-kit^{+} cells detected in the Kit^{W}/Kit^{W-v} did not express the Ki67 cycling antigen as frequently as those in wild-type mice (Figure 4C).

c-kit dysfunction increases apoptosis and decreases mitogenesis. Next, to understand the mechanism of cardiac failure in Kit^{W}/Kit^{W-v} mice, we evaluated surrogate measures of cellular proliferation and apoptosis. Nearly 15% of nuclei in wild-type mice expressed Ki67 in the infarct border zone on day 7 after MI (Figure 4, G and H). Previous studies have suggested that the majority of the cycling cells in infarcted myocardium are cardiac endothelial cells and myofibroblasts but not the recruited leukocytes (22). Interestingly, we observed that the percentage of cells that expressed the cycling antigen Ki67 in the border zone and the remote myocardium was significantly diminished in the Kit^{W}/Kit^{W-v} mice (Figure 4, G and H). At most, only 0.14% of cardiomyocytes coexpressed Ki67 in $Kit^{+/+}$ mice, ruling out the possibility that absent cardiomyocyte regeneration played a potential role in the cardiomyopathic phenotype of Kit^{W}/Kit^{W-v} mice. Plotting the number of infiltrating c-kit^{+} cells against the number of cells expressing Ki67 in the border zone showed a linear correlation (Figure 4I). Evaluation of the rate of apoptotic cell death by a TUNEL assay also showed a difference at day 7, with a lower apoptosis rate in the $Kit^{+/+}$ mice (Figure 4, J and K). Thus, greater c-kit^{+} cell infiltration was associated with increased mitogenesis and decreased apoptosis in particular in the infarct border zone 7 days after MI.

c-kit dysfunction is associated with abnormal EPC mobilization and function. To trace back the diminished c-kit^{+} cell infiltration in the Kit^{W}/Kit^{W-v} mice to the bone marrow, we evaluated the impact of MI on mobilization of c-kit^{+} cells into the peripheral circulation. We used 3 independent assays that included quantification of the number of hematopoietic progenitor cells by a semisolid methylcellulose CFU assay, quantification of the number of VEGFR2^{+} cells by flow cytometry, and quantification of the number of EPCs by the fibronectin adhesion assay. MI in $Kit^{+/+}$ mice rapidly increased the number of circulating VEGFR2^{+} cells, circulating EPCs, and circulating hematopoietic CFCs (Figure 5, A–C). In Kit^{W}/Kit^{W-v} mice, no increase in the number of such cells was observed ($P < 0.05$ for all 3 experiments) (Figure 5, A–C).

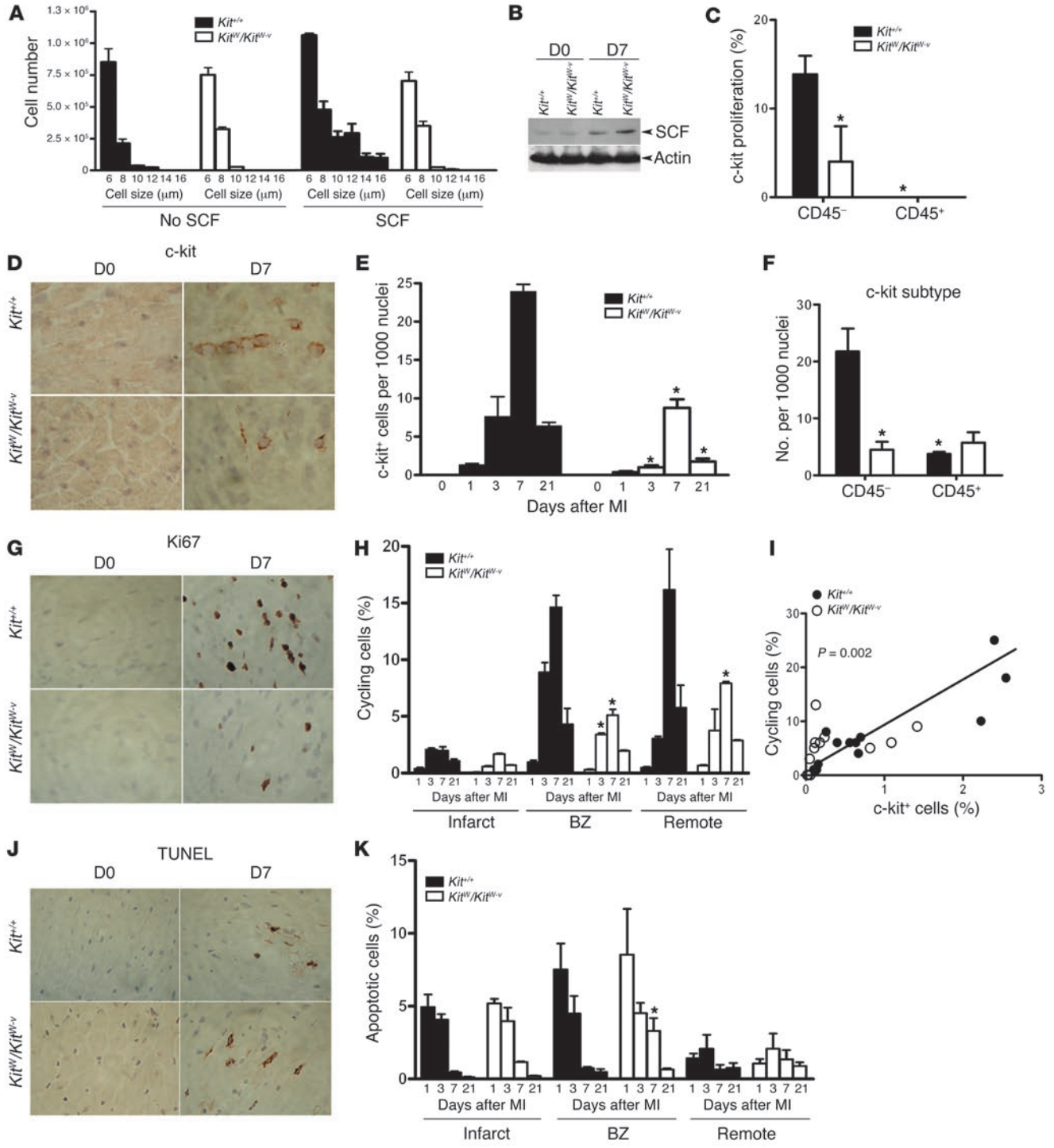

Figure 4

c-kit dysfunction increases apoptosis and decreases mitogenesis. (**A**) Incubation of bone marrow cells from *Kit*$^{+/+}$ mice with 50 ng/ml of recombinant SCF causes cell proliferation. *Kit*^{W}/*Kit*$^{W-v}$ bone marrow cells had no response to SCF. (**B**) After coronary ligation, myocardial SCF levels increased in both *Kit*$^{+/+}$ and *Kit*^{W}/*Kit*$^{W-v}$ mice. Representative immunoblot of 5 independent experiments is shown. (**C**) Consistent with the in vitro data, the recruited c-kit^{+} cells in *Kit*^{W}/*Kit*$^{W-v}$ mice had lower index of proliferation as assessed by Ki67 and c-kit staining and visualized by confocal microscopy of 10 random ×400 fields. $n = 3$ per group. $^{*}P < 0.05$. (**D**) The total number of c-kit^{+} cells in *Kit*^{W}/*Kit*$^{W-v}$ mice was lower than in *Kit*$^{+/+}$ mice. (**E**) Quantification of the total number of c-kit–expressing cells in the infarcted myocardium. $n = 3$ per time point per group. (**F**) The *Kit*$^{+/+}$ mice had more CD45^{-} c-kit^{+} cells than *Kit*^{W}/*Kit*$^{W-v}$ mice. $n = 3$ per group. (**G**) Nonmyocyte mitogenesis was markedly higher in *Kit*$^{+/+}$ mice in the infarct border zone. (**H**) Quantification of general mitogenesis by region and over a time course. $n = 3$ per time point per group. $^{\#}P < 0.01$. BZ, border zone. (**I**) The number of infiltrating c-kit–expressing cells correlated with the number of cycling cells ($r = 0.78$). (**J**) Differences in apoptotic cell death as quantified in **K** were smaller than differences in mitogenesis. $n = 3$ per time point per group. $^{*}P < 0.05$ versus *Kit*$^{+/+}$. Magnification, ×200.

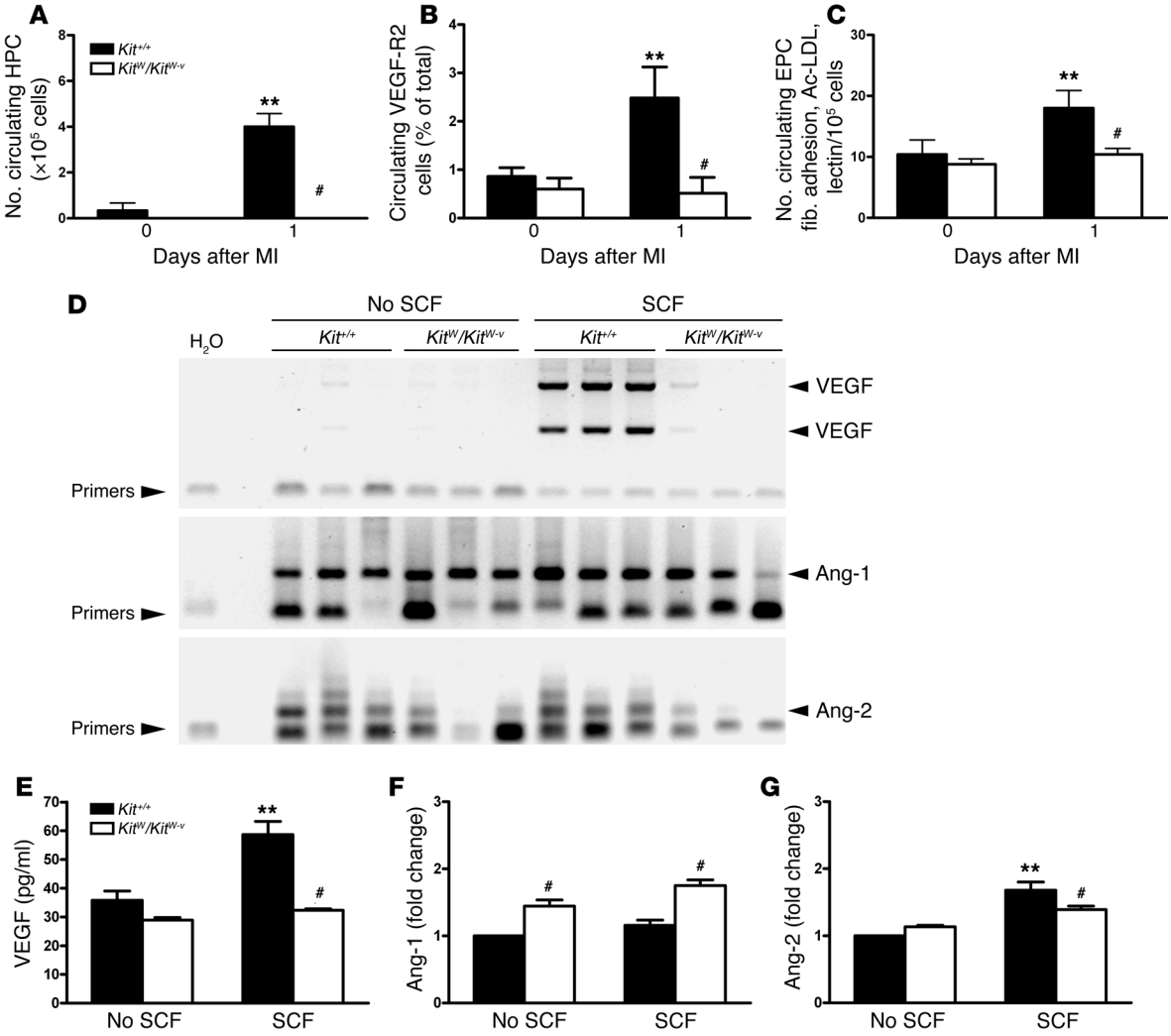

Figure 5

c-kit dysfunction is associated with abnormal EPC mobilization and function. (**A**–**C**) c-kit function is required for the mobilization of hematopoietic progenitor cells (HPC), VEGFR2+ PBMCs, and EPCs after MI ($n = 5$ per group). $^{**}P < 0.05$ versus Day 0 values; $^{\#}P < 0.05$ versus $Kit^{+/+}$. (**D**) RT-PCR reaction for VEGF, angiopoietin-1 (Ang-1), and angiopoietin-2 from bone marrow cells of $Kit^{+/+}$ or Kit^{W}/Kit^{W-v} mice cultured for 7 days in the absence or presence of recombinant SCF. SCF led to marked-up regulation of VEGF mRNA only in $Kit^{+/+}$ mice. Angiopoietin-2 levels were higher in $Kit^{+/+}$ mice. (**E**–**G**) Quantification of VEGF by ELISA and angiopoietin-2 and angiopoietin-1 levels by immunoblotting and densitometry from cell supernatant described above. SCF caused increased VEGF and higher angiopoietin-2/angiopoietin-1 ratio only in $Kit^{+/+}$ mice. The values are from 3 independent experiments quantified in triplicate. $^{**}P < 0.05$ versus no SCF values; $^{\#}P < 0.05$ versus $Kit^{+/+}$.

To test the c-kit–dependent proangiogenic functionality of bone marrow cells isolated from $Kit^{+/+}$ and Kit^{W}/Kit^{W-v} mice, we cultured whole bone marrow cells from the 2 types of mice in the presence or absence of SCF. In $Kit^{+/+}$ cells, coincubation with SCF resulted in marked upregulation of the VEGF mRNA (Figure 5D). Angiopoietin-1 was expressed by both groups and was not induced by incubation with SCF (Figure 5D). Angiopoietin-2 was expressed at higher levels in the $Kit^{+/+}$ bone marrow cells (Figure 5D). Enzyme-linked immunosorbent measurement of VEGF levels in the supernatant confirmed that $Kit^{+/+}$ cells incubated with SCF produced highest levels of VEGF (Figure 5E). Immunoblotting also showed greater angiopoietin-2 production in the $Kit^{+/+}$ and greater angiopoietin-1 production in the Kit^{W}/Kit^{W-v} bone marrow cells (Figure 5, F and G). Thus, proangiogenic cytokine oscillations may be induced by SCF in bone marrow cells only if the c-kit receptor is functional, and c-kit functionality is critical for the mobilization of c-kit+ cells to the blood and heart after MI.

c-kit dysfunction limits myocardial angiogenesis and formation of repair tissue. We next examined the balance of angiogenic cytokines within the infarcted heart to evaluate the influence of bone marrow c-kit+ cell mobilization on endothelial mitogenesis and angiogenesis. Seven days after MI, $Kit^{+/+}$ hearts had an upregulation of VEGF that was principally immunolocalized to the border zone (Figure 6, A–C). Concomitantly, myocardial levels of angiopoietin-2 were increased relative to angiopoietin-1 (Figure 6, D–F). In the Kit^{W}/Kit^{W-v} mice, myocardial VEGF levels were high at baseline, but there was no further increase after coronary ligation (Figure 6A), and no targeting of VEGF to the infarct border zone was evident (Figure 6, B and C). In contrast to $Kit^{+/+}$ mice, which had a pattern similar to that of angiopoietin expression in other studies

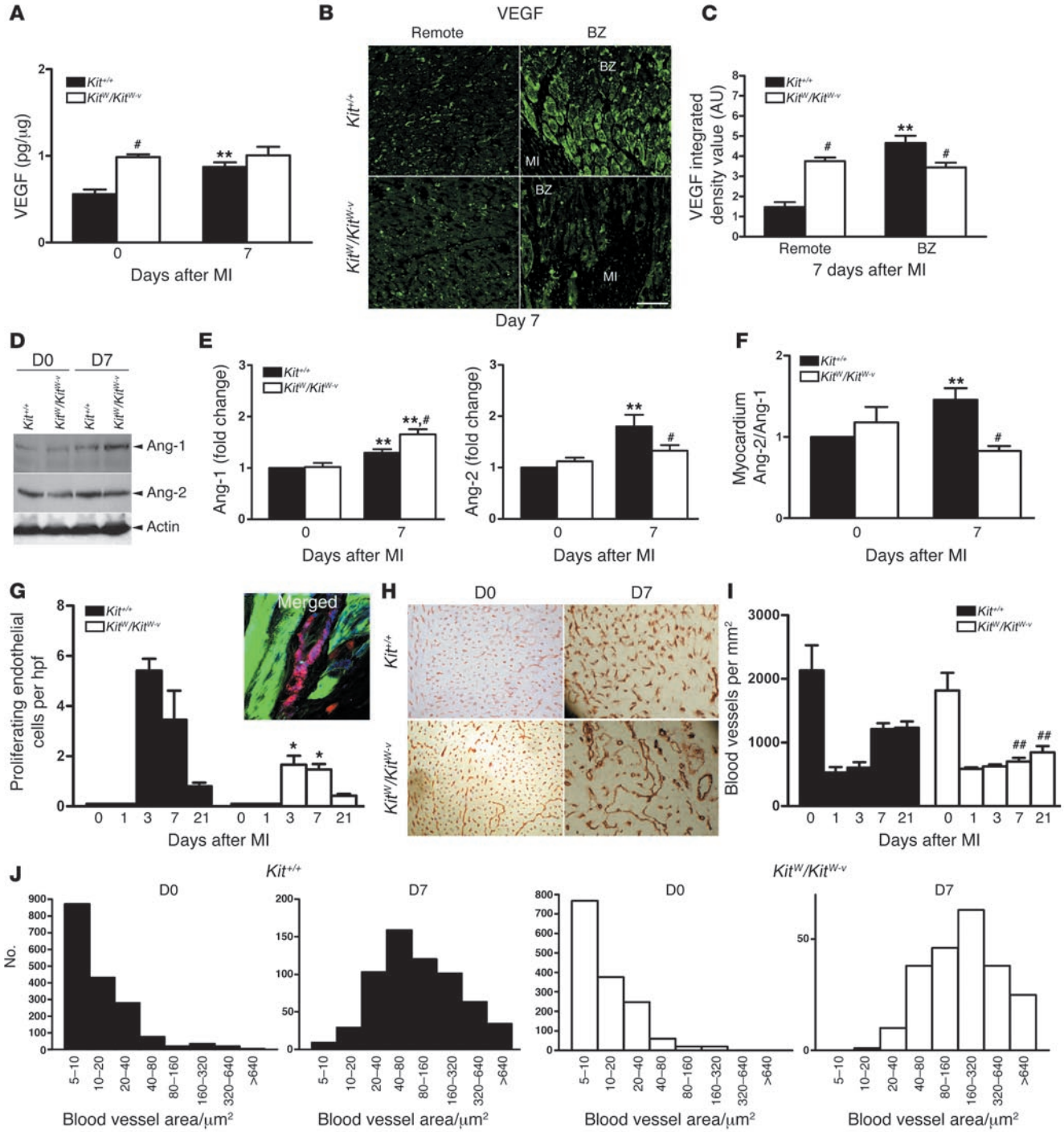

Figure 6

c-kit dysfunction limits myocardial angiogenesis. (**A**) VEGF upregulation by total heart ELISA following MI is abrogated in Kit^{W}/Kit^{W-v} mice. $n = 5$ per group. (**B**) The VEGF in the Kit^{W}/Kit^{W-v} mouse myocardium is diffusely present and is not localized to the border zone, as quantified in **C**. $n = 4$ per group. (**C**) Integrated density value determined by random sampling in 3 ×400 fields per animal. $n = 4$ per group. (**D** and **E**) $Kit^{+/+}$ responds to MI by increasing the ratio of angiopoietin-2 to angiopoietin-1 whereas Kit^{W}/Kit^{W-v} responds in the opposite fashion. Representative immunoblot is shown. Data are quantified by immunoblotting and densitometry from 4 independent experiments in triplicates. (**F**) Angiopoietin-2/angiopoietin-1 ratio. $^{**}P < 0.05$ versus day 0 (D0) values; $^{\#}P < 0.05$ versus $Kit^{+/+}$. (**G**) Number of endothelial cells (blue is CD31) in the cell cycle (red is Ki67) was quantified using confocal microscopy (actin is green) in 5 random ×400 fields in the border zone. $n = 3$ per group per time point. Number of cycling endothelial cells, which appear magenta in color because of overlap of blue CD31 and red Ki67 staining, was higher in the $Kit^{+/+}$ mice. $^{*}P < 0.05$. hpf, high-power field. (**H**) Blood vessel density was assessed by CD31 immunohistochemistry in the border zone. (**I**) Quantification of the number of $CD31^{+}$ structures from 5 random ×400 fields converted to mm^2 showing diminished angiogenic response in Kit^{W}/Kit^{W-v} mice. $^{\#\#}P < 0.01$. (**J**) Blood vessel size quantification showing the Kit^{W}/Kit^{W-v} mice vessels to be fewer and of larger caliber. $n = 5$ per group.

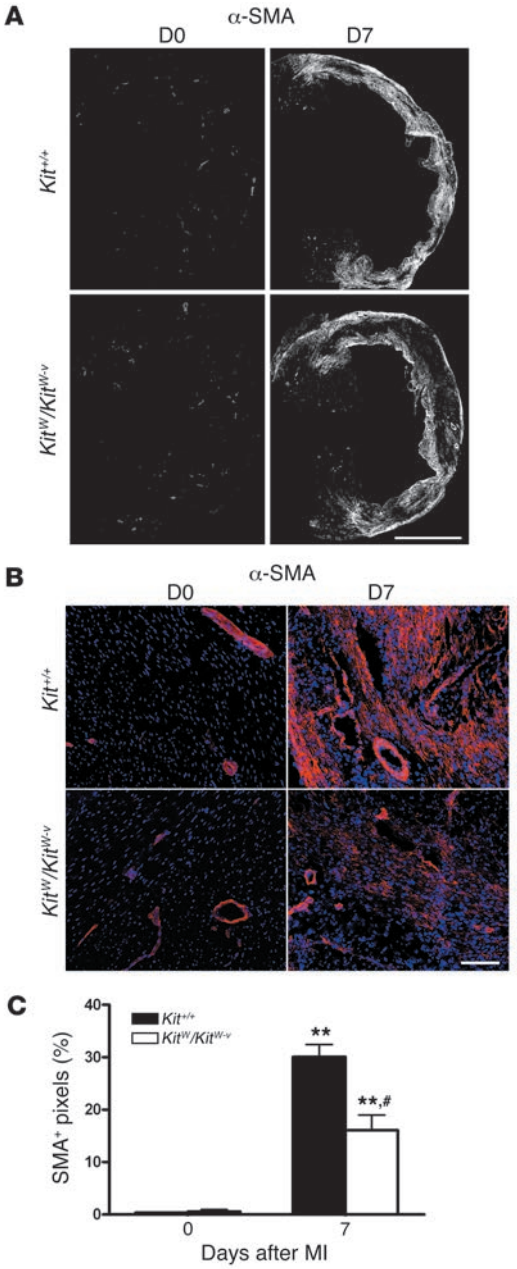

Figure 7
c-kit dysfunction limits the formation of repair tissue. (**A**) Representative composite images constructed from 15–20 ×10 magnification images demonstrates less α-SMA per infarct area in Kit^{W}/Kit^{W-v} 7 days after MI when compared with $Kit^{+/+}$ mice. (**B**) Higher magnification images of the border zone and scar area demonstrate that the majority of α-SMA–positive cells are localized in the scar region. (**C**) Quantitative morphometrical analysis shows a significant difference between the strains. $n = 3$ per group per time point. $^{**}P < 0.05$ versus day 0 values; $^{\#}P < 0.01$ versus $Kit^{+/+}$.

(23), the angiopoietin-2 levels were decreased relative to angiopoietin-1 in the Kit^{W}/Kit^{W-v} mice (Figure 6, D–F). Thus, reversal of angiopoietin ratios in favor of angiopoietin-2, which is necessary for release of the endothelial cells from quiescence (24), and the microenvironmental increase in border-zone VEGF (25) were both absent in Kit^{W}/Kit^{W-v} mice.

Considering the proangiogenic milieu established in the $Kit^{+/+}$ border zone compared with the Kit^{W}/Kit^{W-v} mice, we evaluated endothelial mitogenesis and found that a greater number of endothelial cells appeared to be in the cell cycle in the $Kit^{+/+}$ than the Kit^{W}/Kit^{W-v} mice by double immunofluorescence quantification of $CD31^{+}$ cells that expressed Ki67 in their nuclei (Figure 6G). Accordingly, after a day 1 nadir following ligation, the number of border-zone blood vessels was increased in the $Kit^{+/+}$ mice as compared with the Kit^{W}/Kit^{W-v} group (Figure 6, H and I). Morphometry demonstrated that the $Kit^{+/+}$ blood vessels in the border zone were smaller in caliber and more similar to capillaries, suggestive of sprouting angiogenesis, in contrast to the markedly enlarged and fewer blood vessels in the Kit^{W}/Kit^{W-v} mice (Figure 6J).

The onset of angiogenesis was closely correlated with repopulation of the infarcted segment with α-SMA–expressing myofibroblasts in $Kit^{+/+}$ mice (Figure 7, A–C). Specifically, the percentage of the scar occupied by α-SMA–expressing cells was 30.1% ± 4.1% in $Kit^{+/+}$ mice compared with 16.1% ± 5.1% in the Kit^{W}/Kit^{W-v} mice ($P < 0.01$) (Figure 7D) 7 days after MI. Thus, the formation of granulation tissue composed of myofibroblasts and blood vessels, which is a critical aspect of cardiac repair after MI, was significantly attenuated when c-kit was dysfunctional.

Bone marrow rescue also rescues the cardiomyopathic phenotype. Lastly, given that the majority of the $c\text{-}kit^{+}$ cells in the heart appeared to be from the bone marrow in our chimeric experiments, we evaluated whether the cardiomyopathic phenotype of the c-kit mutant could be rescued solely by bone marrow rescue of the mutant mice with wild-type bone marrow cells. Chimeric Kit^{W}/Kit^{W-v} mice were engineered whose bone marrow cells were of $Kit^{+/+}$ origin. As a control for the irradiation conditioning protocol used for bone marrow replacement, a subgroup of $Kit^{+/+}$ mice were also irradiated and reinjected with $Kit^{+/+}$ bone marrow cells. Two weeks after coronary ligation, transthoracic echocardiography and invasive hemodynamic measurements confirmed that bone marrow rescue led to the rescue of the dilated cardiomyopathic phenotype in the Kit^{W}/Kit^{W-v} mice. We observed near complete restoration of systolic function and prevention of exaggerated ventricular dilation (Figure 8, A–C). No significant impact of the irradiation protocol was evident in the $Kit^{+/+} \rightarrow Kit^{+/+}$ bone marrow transplantation.

Furthermore, bone marrow rescue increased myocardial VEGF levels to 1.3-fold above those of nonrescued Kit^{W}/Kit^{W-v} mice ($P = 0.01$) (Figure 8, D and E). Similarly, myocardial PCNA expression increased 1.2-fold above that of nonrescued Kit^{W}/Kit^{W-v} mice. Blood vessel count in the infarct border zone showed that bone marrow rescue also resulted in a 1.4-fold increase in the number of blood vessels in the Kit^{W}/Kit^{W-v} border zone 7 days after MI ($P < 0.01$) (Figure 8F). Thus, reconstitution of Kit^{W}/Kit^{W-v} bone marrow with $Kit^{+/+}$ bone marrow rescued the Kit^{W}/Kit^{W-v} cardiomyopathic phenotype at the biochemical, histological, morphometric, and functional levels.

Discussion

Given that c-kit function appears to be required for mobilization of bone marrow $c\text{-}kit^{+}$ HSC, we reasoned that studying mice with attenuated c-kit function would allow us to uncover the role of $c\text{-}kit^{+}$ cells in cardiac repair. We found in our compound heterozygous c-kit mutant Kit^{W}/Kit^{W-v} mice that MI leads to rapid dilated cardiomyopathy and poor survival, a phenotype that was

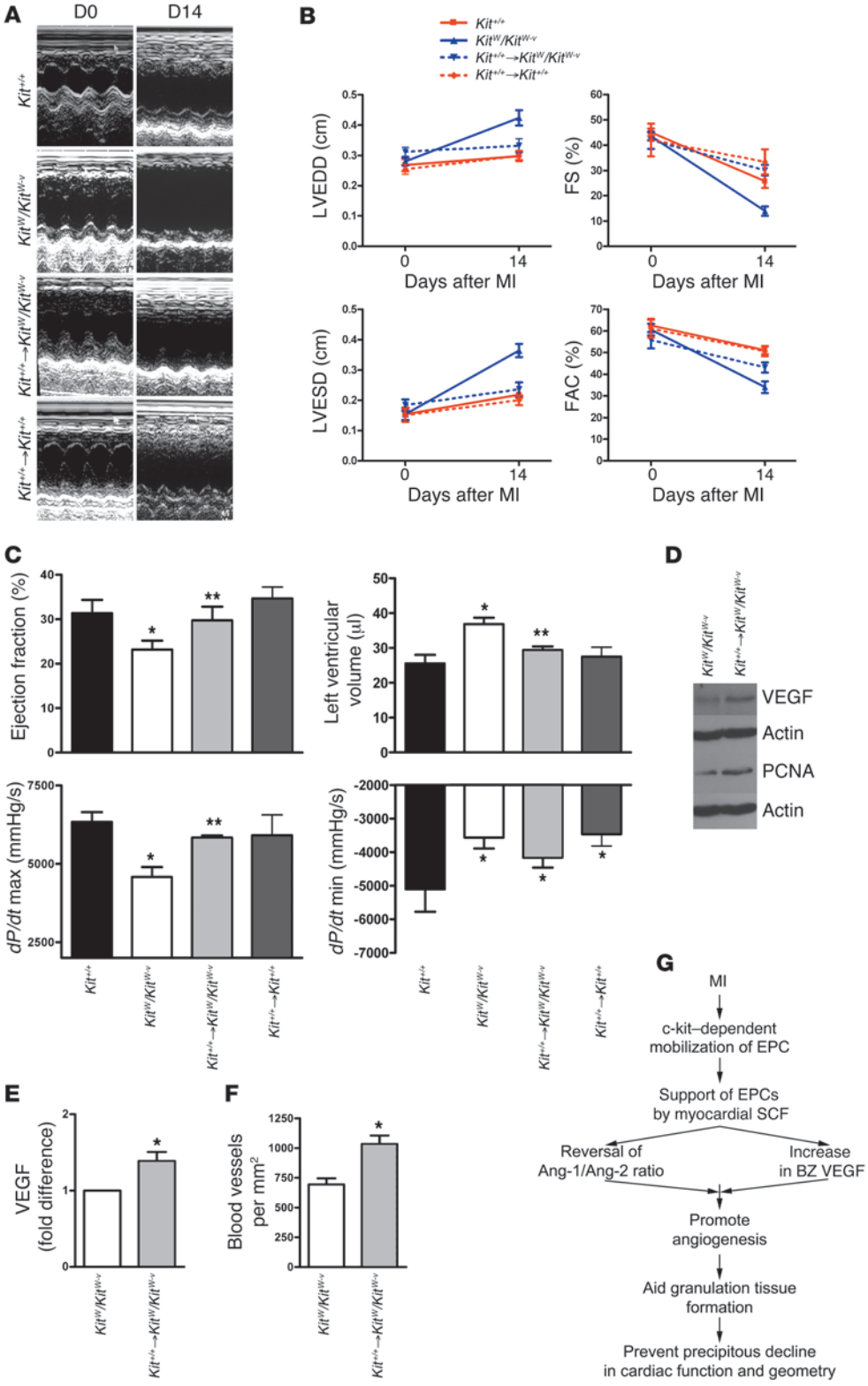

Figure 8
Bone marrow rescue also rescues the cardiomyopathic phenotype. (**A**) Representative M-mode echocardiographic images in $Kit^{+/+}$, Kit^{W}/Kit^{W-v}, and Kit^{W}/Kit^{W-v} mice whose bone marrow was rescued by $Kit^{+/+}$ bone marrow after lethal irradiation ($Kit^{+/+} \rightarrow Kit^{W}/Kit^{W-v}$) and $Kit^{+/+}$ mice who received the same dose of irradiation and whose bone marrow was reconstituted from other $Kit^{+/+}$ mice ($Kit^{+/+} \rightarrow Kit^{+/+}$), showing the prevention of ventricular dilation in $Kit^{+/+} \rightarrow Kit^{W}/Kit^{W-v}$ mice. (**B**) Quantification of echocardiographic parameters: left ventricular end-diastolic diameter (LVEDD), left ventricular end-systolic diameter (LVESD), fractional shortening (FS), and fractional area contraction (FAC). $n = 5$ per group. Bone marrow rescue prevented ventricular dilation and better preserved ventricular systolic function. (**C**) Invasive hemodynamic measurements 2 weeks after coronary ligation. Bone marrow rescue also rescued parameters of systolic function, such as ejection fraction and dP/dt maximum (max), and prevented ventricular dilation, but did not affect dP/dt minimum (min). $n = 5$–7 per group. $^{*}P < 0.05$ versus $Kit^{+/+}$; $^{**}P < 0.05$ versus Kit^{W}/Kit^{W-v}. (**D**) Bone marrow rescue results in higher myocardial VEGF levels and greater cell cycle activity (PCNA expression). The immunoblots are representative of 4 independent experiments. (**E**) Quantification of myocardial VEGF from 4 independent experiments performed in triplicate. (**F**) Bone marrow rescue increases border-zone blood vessels. $n = 5$–7 per group. $^{*}P < 0.05$ versus Kit^{W}/Kit^{W-v} (**E** and **F**). (**G**) Recruitment of c-kit^{+} cells from the bone marrow to the injured region of the heart is cardioprotective because it regulates the myocardial balance of angiogenic cytokines.

recapitulated in mice in which c-kit was rendered acutely dysfunctional by Gleevec. However, Gleevec also antagonizes Abl, which is important to compact-layer expansion during cardiac development (26), phosphorylates the Z-disk protein ArgBP2 (27), and may affect cardiac function in a c-kit–independent manner. In spite of these considerations, the results of the 2 separate experiments are consistent with the notion that c-kit function is important to cardiac repair.

We also addressed the source of the majority of the c-kit^{+} cells that are recruited to the infarcted heart. This is important because

c-kit may also define a new cardiac-specific stem cell (8) and abnormalities in this cell type may account for part of our observations. The cardiac specificity of the c-kit$^+$ cells isolated from the heart was previously concluded from the absence of the pan-hematopoietic cell-surface marker CD45 on the cells. But CD45 downregulation in that subset was not ruled out. In fact, CD45 downregulation may be necessary for cellular activation (28–30). To address this issue, we constructed chimeric mice whose bone marrow cells were donated from GFP transgenic animals. Interestingly, we observed that the majority of the c-kit$^+$ cells in the heart carried the GFP transgene, strongly suggesting that the cells were of bone marrow origin. Although we did not show that the multipotent and clonogenic c-kit$^+$ cells isolated from the heart are from the bone marrow, our results raise the possibility that the putative cardiac c-kit$^+$ stem cells are in actuality not from the heart. This observation would parallel findings in skeletal muscle tissue where muscle resident stem cells were tracked back to a bone marrow origin (31).

We also observed that the recruitment of bone marrow c-kit$^+$ cells was correlated with mitogenesis of noncardiomyocytes, suggesting that the recruited c-kit$^+$ cells express mitogens, consistent with the prevailing view of the role of c-kit$^+$ EPCs with regard to endothelial cells (32–34). In our study, post-MI angiogenesis was severely impaired in mice with abnormal c-kit function. This observation is also consistent with previous evidence (11, 18, 19, 35–37). Importantly, administration of intravenous SCF to wild-type mice can improve post-MI angiogenesis, suggesting that this pathway may be overdriven to improve neovascularization (38). In the present series of experiments, we also showed that whereas the wild-type mice generated more than 700 blood vessels per mm^2 in the peri-infarct border zone, the Kit^W/Kit^{W-v} mice generated only 60 blood vessels per mm^2, and this deficiency was corrected by prior transplantation of $Kit^{+/+}$ bone marrow cells.

Normal c-kit function was associated with border zone–specific increase in VEGF that was accompanied by a reversal of angiopoietin-2/angiopoietin-1 ratio in favor of angiopoietin-2. Angiopoietin-2 is critical in postnatal angiogenesis because it blocks the tonic quiescent signal that is delivered by angiopoietin-1. Increased angiopoietin-2/angiopoietin-1 ratio potentiates the endothelial cells' responsiveness to VEGF and promotes blood vessel sprouting (24). Our blood vessel morphology data are reminiscent of findings in a cornea micropocket angiogenesis assay (39). In that study, VEGF in the presence of excess angiopoietin-1 resulted in the formation of fewer neovessels that were large in caliber, and VEGF in the presence of excess angiopoietin-2 resulted in the formation of a much greater number of smaller vessels of longer length (39). Taken together, our data suggest that in infarcted myocardium, c-kit$^+$ cells are required to mediate the important transition of quiescent to active endothelium, which has been coined as the cytokine-mediated angiogenic switch in tumorigenesis (40, 41).

Indeed, bone marrow–derived c-kit$^+$ cells act as the angiogenic switch in tumors, and blocking c-kit signaling blocks tumor angiogenesis (18–20). Of particular importance to our study, the Kit^W/Kit^{W-v} mice are also unable to activate their quiescent vasculature even in the setting of forced epithelial carcinogenesis (18). Considering the role of c-kit signaling in mobilization of EPCs (16, 17), as also documented in our present study, it is conceivable that this angiogenic switch, partially or in whole, is mediated by the EPCs that are rapidly recruited to sites of physiologic and pathologic angiogenesis (42). During the preparation of this manuscript, Heissig et al. also noted an absence of EPC mobilization in the Sl/Sl^d mouse, which bears mutations in the c-kit ligand (SCF) in response to hind-limb ischemia, further supporting the observations in the present report (43). Furthermore, Gleevec is also known to suppresses VEGF secretion and limit sprouting angiogenesis (44, 45), consistent with our series of observations.

Angiogenesis is an important aspect of granulation repair tissue. Infarcted segment stabilization is mediated by the abundant myofibroblast-rich tissue that forms rapidly in the scar (22). The Kit^W/Kit^{W-v} mice had poor formation of smooth-muscle actin expressing granulation tissue. An inability to provide the vascular support for the granulation tissue may explain the exaggerated ventricular dilation after MI in Kit^W/Kit^{W-v} mice (46) although a primary defect in the myofibroblast proliferation or differentiation cannot be ruled out. Interestingly, the Kit^W/Kit^{W-v} mice are protected from diastolic failure induced by pressure overload–mediated cardiac fibrosis (47). The principal mediator of cardiac fibrosis is the myofibroblast population. Interference with formation of myofibroblast-rich tissue, therefore, may account for the seemingly opposing observations. Protection from pressure overload also highlights that the principle deficiency of the Kit^W/Kit^{W-v} mice is unlikely to be at the cardiac progenitor/stem or cardiomyocyte level because such a deficiency would be predicted to be detrimental under both experimental cardiac injuries.

The protection in the mutant mice in the aortic banding model was mostly attributed to the known mast cell deficiency of the Kit^W/Kit^{W-v} mice. Surprisingly, in our model system, very few mast cells were present in the infarcted hearts at a time when various other parameters were most divergent between the 2 groups of mice. Furthermore, the majority of the c-kit$^+$ cells did not show evidence for containing mast cell–specific granules, and the few mast cells that were present in the bone marrow chimeric GFP mice did not appear to carry the GFP transgene. The latter observation suggests that mast cells that home to the infarcted heart do not arise from bone marrow progenitors within the 4-week time frame from the bone marrow transplantation to coronary ligation. Coupled with our finding that bone marrow transplantation in the Kit^W/Kit^{W-v} mice within the same time frame rescues the cardiomyopathic phenotype, the data suggest that mast cells are unlikely to be major players in cardiac repair in the 2-week period following an MI in the mouse heart.

In summary, we believe that the activation of the c-kit receptor on bone marrow–derived cells is important for their mobilization to the infarcted heart, where the cells act to initiate angiogenesis and potentiate the formation of myofibroblast-rich repair tissue (Figure 8G). Given that the cells are able to modify cardiac repair without the requirement to engraft in the heart over the long term, a unique therapeutic window is apparent. Bone marrow senescence in patients with coronary artery disease may partially underlie the inefficient cardiac repair that eventually leads to congestive heart failure in these patients. Transplantation of bone marrow cells prepared from young allogenic donors may significantly enhance cardiac repair, in particular because only temporary engraftment of the cells is required.

Methods

For a list of materials, antibody clone information and manufacturers, and more detailed protocols, please see the Supplemental Methods.

Mice. Eight- to ten-week-old female C57BL/6, WBB6F$_1$-Kit^W/Kit^{W-v}, and $Kit^{+/+}$ congenic controls, and C57BL/6-TgN(ACTbEGFP)1Osb enhanced GFP transgenic mice were from Jackson Laboratory. The C57BL/6-TgN(ACTbEGFP)1Osb hemizygote mouse has the chicken cytoplasmic

β-actin promoter with the cytomegalovirus enhancer elements driving the expression of an enhanced GFP cDNA. All tissues, with the exception of erythrocytes and hair, fluoresce under excitation light (48).

Animal procedures. The Animal Care Committee of the University Health Network approved all experimental procedures, which were in accordance with the National Research Council's *Guide for the Care and Use of Laboratory Animals* (49). Animals were intubated and ventilated with 2% isoflurane. Through a thoracotomy, the left coronary artery was ligated. To control for the anemia of the Kit^{W}/Kit^{W-v} mice, acute hemodilution of the C57BL/6 mice was performed after coronary ligation with aspiration of 15% of blood volume from the jugular vein. We injected 2 × 1 ml of normal saline intraperitoneally before and after the procedure. The mortality for combined MI and hemodilution was 64%. Gleevec was begun 2 days prior to MI, and 10 mg/kg was administered twice a day by oral gavage to the end of the study. For bone marrow reconstitution, mice were irradiated (9.5 Gy). We injected 2.5×10^7 fresh bone marrow cells from donors prepared in aseptic fashion into the tail vein. After 4–6 weeks, reconstitution was assessed. Determination of myocardial volume excluded from circulation by coronary ligation and infarcted myocardial volume were performed by Evans blue and triphenyltetrazolium chloride staining.

Cardiac function and geometry. Under isoflurane anesthesia, a micromanometer and conductance 1.4 French catheter (SPR-839 Millar Instruments) was introduced into the left ventricle through the right carotid artery. After stabilization, the signals were continuously recorded at a sampling rate of 1000/s using pressure-volume conductance system coupled to a PowerLab/4SP analog to digital converter (ADInstruments). All pressure-volume loops were analyzed by using a cardiac pressure-volume analysis program (PVAN 3.3; Millar Instruments). Echocardiographic recording was performed under ketamine/xylazine sedation using a Sequoia C256 System (Siemens). M-mode and 2D images were obtained in parasternal short axis at the level of the papillary muscles. Cardiac measurements were completed off-line as detailed in the Supplemental Methods.

Forty-two days after MI, hearts were arrested, perfusion-fixed at physiologic pressures using buffered 10% formalin, weighed, cut into 1-mm sections, photographed for morphometric measurements using computerized planimetry, and sectioned for histology.

In vitro experiments. We plated 5×10^5 fresh bone marrow cells from $Kit^{+/+}$ and Kit^{W}/Kit^{W-v} mice in 2 ml of Iscove's Modified Dulbecco's Media supplemented with fetal bovine serum, β-mercaptoethanol, and antibiotics in 6-well plates in the presence or absence of 50 ng/ml of recombinant murine SCF. Cells were incubated for 7 days in humidified 37°C incubators with 5% CO_2 and supplemental oxygen without changing the medium. Cell number and size were assessed by an automated cell counter using incremental size gates (Beckman Coulter). Cells and supernatant were then collected for biochemical analysis.

Microscopy. For determination of cardiac structural features, including measurement of myocyte hypertrophy and evaluation of collagen matrix structure, transverse myocardial sections from hearts perfusion fixed at physiologic pressures were used. For confocal microscopy, frozen sections embedded in OCT compound (Sakura) were used to minimize the autofluorescence of infarcted myocardium.

Flow cytometry. A single-cell suspension of 5×10^5 cells was blocked with 5% BSA, incubated with CD45, c-kit, Sca-1, VEGFR2, or IgG isotype control antibodies (1 μg/10^6 cells), and subjected to flow cytometry using EPICS XL-MCL flow cytometer and Expo32 ADC Xa software (Beckman Coulter).

Immunoblotting and RT-PCR. Immunoblotting was performed as per routine protocol detailed in Supplemental Methods. For quantification, densitometry of the protein band of interest was divided by the corresponding densitometry of the actin band using AlphaImager 2200 software. Reported values were normalized to pre-injury (D0) or to no SCF $Kit^{+/+}$ values, which were arbitrarily assigned the value of 1. For Gleevec dose response, the drug was dissolved at pH 4.0 in water and diluted in Iscove's Modified Dulbecco's Medium to a range of 1 to 100 μM.

Total RNA was extracted from bone marrow cells by TRIZOL reagent as per manufacturer's instructions. RT-PCR was performed using 1 μg of total RNA for 25–35 cycles to ensure amplification in the linear range. The primer sequences are listed in the Supplemental Methods.

Statistics. Data are presented as mean ± SEM. Statistical analysis between 2 groups was carried out using an unpaired 2-tailed nonequal variance Student's *t* test. Time course and multigroup analyses were carried out using ANOVA. Tukey's or Bonferroni's post-test were used to detect data points at which differences between groups reached statistical significance. Survival data were analyzed by Kaplan-Meier survival curves and log-rank statistics. $P < 0.05$ was considered statistically significant.

Acknowledgments

The authors wish to acknowledge the technical assistance of Amy Wong, Jun Wu, and Xing-Hua Wang. This work was supported by Heart and Stroke Foundation (HSF) of Ontario grants (T5287 to R.D. Weisel and S. Fazel), Canadian Institute of Health Research (CIHR) grants (MOP14795 to R.-K. Li and S. Fazel), and a Physician Services Incorporated Foundation grant to S. Fazel. S. Fazel has been awarded a CIHR fellowship and a joint HSF and CIHR TACTICS fellowship. He is also a McLaughlin Centre for Molecular Medicine research fellow. A. Keating holds the Gloria and Seymour Epstein Chair in Cell Therapy and Transplantation at the University of Toronto. R.-K. Li is a career investigator of the HSF and holds a Canada Research Chair in cardiac regeneration.

Received for publication October 3, 2005, and accepted in revised form April 25, 2006.

Address correspondence to: Ren-Ke Li, NU 1-115, 200 Elizabeth Street, Toronto General Hospital, Toronto, Ontario M5G-2C4, Canada. Phone: (416) 340-3361; Fax: (416) 340-4806; E-mail: renkeli@uhnres.utoronto.ca.

1. Orlic, D., et al. 2001. Mobilized bone marrow cells repair the infarcted heart, improving function and survival. *Proc. Natl. Acad. Sci. U. S. A.* **98**:10344–10349.
2. Orlic, D., et al. 2001. Bone marrow cells regenerate infarcted myocardium. *Nature.* **410**:701–705.
3. Fazel, S., et al. 2005. Current status of cellular therapy for ischemic heart disease. *Ann. Thorac. Surg.* **79**:S2238–S2247.
4. Balsam, L.B., et al. 2004. Haematopoietic stem cells adopt mature haematopoietic fates in ischaemic myocardium. *Nature.* **428**:668–673.
5. Murry, C.E., et al. 2004. Haematopoietic stem cells do not transdifferentiate into cardiac myocytes in myocardial infarcts. *Nature.* **428**:664–668.
6. Nygren, J.M., et al. 2004. Bone marrow-derived hematopoietic cells generate cardiomyocytes at a low frequency through cell fusion, but not transdifferentiation. *Nat. Med.* **10**:494–501.
7. Chabot, B., Stephenson, D.A., Chapman, V.M., Besmer, P., and Bernstein, A. 1988. The proto-oncogene c-kit encoding a transmembrane tyrosine kinase receptor maps to the mouse W locus. *Nature.* **335**:88–89.
8. Beltrami, A.P., et al. 2003. Adult cardiac stem cells are multipotent and support myocardial regeneration. *Cell.* **114**:763–776.
9. Kabrun, N., et al. 1997. Flk-1 expression defines a population of early embryonic hematopoietic precursors. *Development.* **124**:2039–2048.
10. Nishikawa, S.I., Nishikawa, S., Hirashima, M., Matsuyoshi, N., and Kodama, H. 1998. Progressive lineage analysis by cell sorting and culture identifies FLK1+VE-cadherin+ cells at a diverging point of endothelial and hemopoietic lineages. *Development.* **125**:1747–1757.
11. Asahara, T., et al. 1997. Isolation of putative progenitor endothelial cells for angiogenesis. *Science.* **275**:964–967.
12. Rafii, S., and Lyden, D. 2003. Therapeutic stem and progenitor cell transplantation for organ vascularization and regeneration. *Nat. Med.* **9**:702–712.
13. Ikuta, K., and Weissman, I.L. 1992. Evidence that

hematopoietic stem cells express mouse c-kit but do not depend on steel factor for their generation. *Proc. Natl. Acad. Sci. U. S. A.* **89**:1502–1506.
14. Fleming, W.H., Alpern, E.J., Uchida, N., Ikuta, K., and Weissman, I.L. 1993. Steel factor influences the distribution and activity of murine hematopoietic stem cells in vivo. *Proc. Natl. Acad. Sci. U. S. A.* **90**:3760–3764.
15. Papayannopoulou, T., Priestley, G.V., and Nakamoto, B. 1998. Anti-VLA4/VCAM-1-induced mobilization requires cooperative signaling through the kit/mkit ligand pathway. *Blood.* **91**:2231–2239.
16. Heissig, B., et al. 2002. Recruitment of stem and progenitor cells from the bone marrow niche requires MMP-9 mediated release of kit-ligand. *Cell.* **109**:625–637.
17. Heissig, B., Werb, Z., Rafii, S., and Hattori, K. 2003. Role of c-kit/Kit ligand signaling in regulating vasculogenesis. *Thromb. Haemost.* **90**:570–576.
18. Coussens, L.M., et al. 1999. Inflammatory mast cells up-regulate angiogenesis during squamous epithelial carcinogenesis. *Genes Dev.* **13**:1382–1397.
19. Starkey, J.R., Crowle, P.K., and Taubenberger, S. 1988. Mast-cell-deficient W/Wv mice exhibit a decreased rate of tumor angiogenesis. *Int. J. Cancer.* **42**:48–52.
20. Okamoto, R., et al. 2005. Hematopoietic cells regulate the angiogenic switch during tumorigenesis. *Blood.* **105**:2757–2763.
21. Nocka, K., et al. 1990. Molecular bases of dominant negative and loss of function mutations at the murine c-kit/white spotting locus: W37, Wv, W41 and W. *EMBO J.* **9**:1805–1813.
22. Virag, J.I., and Murry, C.E. 2003. Myofibroblast and endothelial cell proliferation during murine myocardial infarct repair. *Am. J. Pathol.* **163**:2433–2440.
23. Sandhu, R., et al. 2004. Reciprocal regulation of angiopoietin-1 and angiopoietin-2 following myocardial infarction in the rat. *Cardiovasc. Res.* **64**:115–124.
24. Hanahan, D. 1997. Signaling vascular morphogenesis and maintenance. *Science.* **277**:48–50.
25. Li, J., et al. 1996. VEGF, flk-1, and flt-1 expression in a rat myocardial infarction model of angiogenesis. *Am. J. Physiol.* **270**:H1803–H1811.
26. Toyofuku, T., et al. 2004. Guidance of myocardial patterning in cardiac development by Sema6D reverse signalling. *Nat. Cell Biol.* **6**:1204–1211.
27. Wang, B., Golemis, E.A., and Kruh, G.D. 1997. ArgBP2, a multiple Src homology 3 domain-containing, Arg/Abl-interacting protein, is phosphorylated in v-Abl-transformed cells and localized in stress fibers and cardiocyte Z-disks. *J. Biol. Chem.* **272**:17542–17550.
28. Irie-Sasaki, J., et al. 2001. CD45 is a JAK phosphatase and negatively regulates cytokine receptor signalling. *Nature.* **409**:349–354.
29. Oliveira, D.M., and Goodell, M.A. 2003. Transient RNA interference in hematopoietic progenitors with functional consequences. *Genesis.* **36**:203–208.
30. Jang, Y.Y., Collector, M.I., Baylin, S.B., Diehl, A.M., and Sharkis, S.J. 2004. Hematopoietic stem cells convert into liver cells within days without fusion. *Nat. Cell Biol.* **6**:532–539.
31. McKinney-Freeman, S.L., et al. 2002. Muscle-derived hematopoietic stem cells are hematopoietic in origin. *Proc. Natl. Acad. Sci. U. S. A.* **99**:1341–1346.
32. Urbich, C., et al. 2005. Soluble factors released by endothelial progenitor cells promote migration of endothelial cells and cardiac resident progenitor cells. *J. Mol. Cell. Cardiol.* **39**:733–742.
33. Galli, S.J., et al. 1992. Analyzing mast cell development and function using mice carrying mutations at W/c-kit or Sl/MGF (SCF) loci. *Ann. N. Y. Acad. Sci.* **664**:69–88.
34. Urbich, C., and Dimmeler, S. 2004. Endothelial progenitor cells: characterization and role in vascular biology. *Circ. Res.* **95**:343–353.
35. Li, T.S., et al. 2003. CD117+ stem cells play a key role in therapeutic angiogenesis induced by bone marrow cell implantation. *Am. J. Physiol. Heart Circ. Physiol.* **285**:H931–H937.
36. Vajkoczy, P., et al. 2003. Multistep nature of microvascular recruitment of ex vivo-expanded embryonic endothelial progenitor cells during tumor angiogenesis. *J. Exp. Med.* **197**:1755–1765.
37. Wojakowski, W., et al. 2004. Mobilization of CD34/CXCR4+, CD34/CD117+, c-met+ stem cells, and mononuclear cells expressing early cardiac, muscle, and endothelial markers into peripheral blood in patients with acute myocardial infarction. *Circulation.* **110**:3213–3220.
38. Kuhlmann, M.T., et al. 2006. G-CSF/SCF reduces inducible arrhythmias in the infarcted heart potentially via increased connexin43 expression and arteriogenesis. *J. Exp. Med.* **203**:87–97.
39. Asahara, T., et al. 1998. Tie2 receptor ligands, angiopoietin-1 and angiopoietin-2, modulate VEGF-induced postnatal neovascularization. *Circ. Res.* **83**:233–240.
40. Hanahan, D., and Folkman, J. 1996. Patterns and emerging mechanisms of the angiogenic switch during tumorigenesis. *Cell.* **86**:353–364.
41. Tait, C.R., and Jones, P.F. 2004. Angiopoietins in tumours: the angiogenic switch. *J. Pathol.* **204**:1–10.
42. Asahara, T., et al. 1999. Bone marrow origin of endothelial progenitor cells responsible for postnatal vasculogenesis in physiological and pathological neovascularization. *Circ. Res.* **85**:221–228.
43. Heissig, B., et al. 2005. Low-dose irradiation promotes tissue revascularization through VEGF release from mast cells and MMP-9-mediated progenitor cell mobilization. *J. Exp. Med.* **202**:739–750.
44. Ebos, J.M., et al. 2002. Imatinib mesylate (STI-571) reduces Bcr-Abl-mediated vascular endothelial growth factor secretion in chronic myelogenous leukemia. *Mol. Cancer Res.* **1**:89–95.
45. Spiekermann, K., Faber, F., Voswinckel, R., and Hiddemann, W. 2002. The protein tyrosine kinase inhibitor SU5614 inhibits VEGF-induced endothelial cell sprouting and induces growth arrest and apoptosis by inhibition of c-kit in AML cells. *Exp. Hematol.* **30**:767–773.
46. Gailit, J., Marchese, M.J., Kew, R.R., and Gruber, B.L. 2001. The differentiation and function of myofibroblasts is regulated by mast cell mediators. *J. Invest. Dermatol.* **117**:1113–1119.
47. Hara, M., et al. 2002. Evidence for a role of mast cells in the evolution to congestive heart failure. *J. Exp. Med.* **195**:375–381.
48. Okabe, M., Ikawa, M., Kominami, K., Nakanishi, T., and Nishimune, Y. 1997. 'Green mice' as a source of ubiquitous green cells. *FEBS Lett.* **407**:313–319.
49. National Research Council. 1996. *Guide for the Care and Use of Laboratory Animals*. Reissue edition. National Academy Press. Washington, DC, USA. 140 pp.